

Anisotropic spin transport and photoresponse characteristics detected by tip movement in magnetic single-molecule junction

Deng-Hui Chen(陈登辉), Zhi Yang(羊志), Xin-Yu Fu(付新宇), Shen-Ao Qin(秦申奥), Yan Yan(严岩), Chuan-Kui Wang(王传奎), Zong-Liang Li(李宗良), and Shuai Qiu(邱帅)

Citation: Chin. Phys. B, 2024, 33 (**4**): 047201. DOI: 10.1088/1674-1056/ad1e65
Journal homepage: http://cpb.iphy.ac.cn; http://iopscience.iop.org/cpb

What follows is a list of articles you may be interested in

Spontaneous isospin polarization and quantum Hall ferromagnetism in a rhombohedral trilayer graphene superlattice

Xiangyan Han(韩香岩), Qianling Liu(刘倩伶), Ruirui Niu(牛锐锐), Zhuangzhuang Qu(曲壮壮), Zhiyu Wang(王知雨), Zhuoxian Li(李卓贤), Chunrui Han(韩春蕊), Kenji Watanabe, Takashi Taniguchi, Zizhao Gan(甘子钊), and Jianming Lu(路建明)

Chin. Phys. B, 2023, 32 (**11**): 117201. DOI: 10.1088/1674-1056/acddcf

Conformational change-modulated spin transport at single-molecule level in carbon systems

Yandong Guo(郭艳东), Xue Zhao(赵雪), Hongru Zhao(赵鸿儒), Li Yang(杨丽), Liyan Lin(林丽艳), Yue Jiang(姜悦), Dan Ma(马丹), Yuting Chen(陈雨婷), and Xiaohong Yan(颜晓红)

Chin. Phys. B, 2022, 31 (**12**): 127201. DOI: 10.1088/1674-1056/ac872d

Current spin polarization of a platform molecule with compression effect

Zhi Yang(羊志), Feng Sun(孙峰), Deng-Hui Chen(陈登辉), Zi-Qun Wang(王子群), Chuan-Kui Wang(王传奎), Zong-Liang Li(李宗良), and Shuai Qiu(邱帅)

Chin. Phys. B, 2022, 31 (**7**): 077202. DOI: 10.1088/1674-1056/ac4f53

Electrically tunable spin diode effect in a tunneling junction of quantum dot

Xukai Peng(彭许凯), Zhengzhong Zhang(张正中)

Chin. Phys. B, 2019, 28 (**12**): 127202. DOI: 10.1088/1674-1056/ab53d0

Recent spinterfacial studies targeted to spin manipulation in molecular spintronic devices

Xian-Rong Gu(谷现荣), Li-Dan Guo(郭立丹), Xiang-Nan Sun(孙向南)

Chin. Phys. B, 2018, 27 (**10**): 107202. DOI: 10.1088/1674-1056/27/10/107202

Anisotropic spin transport and photoresponse characteristics detected by tip movement in magnetic single-molecule junction

Deng-Hui Chen(陈登辉), Zhi Yang(羊志), Xin-Yu Fu(付新宇), Shen-Ao Qin(秦申奥), Yan Yan(严岩), Chuan-Kui Wang(王传奎), Zong-Liang Li(李宗良)[†], and Shuai Qiu(邱帅)[‡]

Shandong Key Laboratory of Medical Physics and Image Processing & Shandong Provincial Engineering and Technical Center of Light Manipulations, School of Physics and Electronics, Shandong Normal University, Jinan 250358, *China*

(Received 12 October 2023; revised manuscript received 1 January 2024; accepted manuscript online 15 January 2024)

Orientation-dependent transport properties induced by anisotropic molecules are enticing in single-molecule junctions. Here, using the first-principles method, we theoretically investigate spin transport properties and photoresponse characteristics in trimesic acid magnetic single-molecule junctions with different molecular adsorption orientations and electrode contact sites. The transport calculations indicate that a single-molecule switch and a significant enhancement of spin transport and photoresponse can be achieved when the molecular adsorption orientation changes from planar geometry to upright geometry. The maximum spin polarization of current and photocurrent in upright molecular junctions exceeds 90%. Moreover, as the Ni tip electrode moves, the tunneling magnetoresistance of upright molecular junctions can be increased to 70%. The analysis of the spin-dependent PDOS elucidates that the spinterfaces between organic molecule and ferromagnetic electrodes are modulated by molecular adsorption orientation, where the molecule in upright molecular junctions yields higher spin polarization. Our theoretical work paves the way for designing spintronic devices and optoelectronic devices with anisotropic functionality base on anisotropic molecules.

Keywords: molecular spintronics, spin polarization, tunneling magnetoresistance, photocurrent, single-molecule junctions

PACS: 72.25.–b, 75.47.–m, 85.75.–d **DOI:** 10.1088/1674-1056/ad1e65

1. Introduction

Molecular spintronics has flourished in recent decades, pointing the way to design and develop low-power, high-performance, and rapidly responsive miniaturized functional devices.[1–4] Compared with conventional inorganic materials, organic molecules have attracted much attention in the regulation of spin transport due to their high chemical plasticity, weak spin–orbit coupling, and long spin relaxation time.[5–8] More importantly, the contact interface between organic molecules and ferromagnetic metals, called spinterface, plays a key role in the spin transport of magnetic single-molecule junction.[9–16] When organic molecules come into contact with ferromagnetic metals, orbital hybridization will occur,[17–19] causing spin polarization (SP) of the molecules and further modulating the SP of current and tunneling magnetoresistance (TMR) of the molecular junction.[20–23] So far, a series of molecular spintronic devices have been devised and fabricated, such as spin rectifiers,[24,25] spin filters,[26,27] spin transistors,[28,29] and spin valves.[30,31] In addition, further consideration of the effect of light field under a magnetic field has led to the emergence of spinphotovoltaic devices,[32–35] which can manipulate the spin transport properties using polarized light.

The commonly used methods for dominating spinterface include changing molecular backbone,[36,37] electrode materials,[38,39] and molecular adsorption configuration relative to the electrode.[40–42] Among them, changing the molecular adsorption configuration is a robust means of controlling the spin-dependent transport properties in single-molecule junctions.[27,43] For example, Li *et al.* achieved an excellent spin filtering effect by stretching the two Ni electrodes to control the tilt angle of benzene ring, disrupting the symmetry of the system.[27] Recently, Afsari *et al.* have designed a single-molecule conductance switch consisting of trimesic acid (TMA) molecule in experiment, where the electrode potential was used to control the adsorption orientation of TMA molecules in the junction from planar (benzene ring plane parallel to the substrate) to upright (benzene ring plane perpendicular to the substrate).[44] A strategy was developed to obtain orientation-dependent anisotropic conductivity in single-molecule junctions by utilizing anisotropic molecules. Therefore, different adsorption orientations of TMA molecules in molecular junction have significant effects on the charge transport capacity. However, the underlying mechanisms of spin-dependent transport properties and photoresponse characteristics mediated by adsorption orientations of TMA molecules in magnetic single-molecule junction are unclear and worthy exploring. It is extremely relevant to facilitate applications of anisotropic molecules in molecular spintronics.

[†]Corresponding author. E-mail: lizongliang@sdnu.edu.cn
[‡]Corresponding author. E-mail: shuaiqiu@sdnu.edu.cn

© 2024 Chinese Physical Society and IOP Publishing Ltd

In this work, we perform a theoretical study on the spin-dependent transport properties and photoresponse characteristics of a magnetic single-molecule junction consisting of a TMA molecule and two ferromagnetic Ni electrodes. The orientation-dependent anisotropic transport properties will be examined by introduced anisotropic molecules. It is found that a conductance switch related to the molecular adsorption orientation is emerged. Meanwhile, the SP of current and photocurrent in junctions with upright molecular adsorption is significantly reinforced owing to high SP of the molecule. In addition, a TMR switch can be manipulated by the contact sites between the TMA molecule and Ni tip electrode, which can be understood from the analysis of transmission spectra and transmission pathways. The remaining parts of this paper are as follows: Section 2 describes the theoretical model and computational details. Section 3 gives the results and discussion. Finally, Section 4 states the conclusions.

2. Theoretical model and computational details

Figure 1 illustrates the theoretical model of a single-molecule junction composed of TMA molecule and Ni electrodes. A TMA molecule is sandwiched between the Ni substrate (bottom electrode) and the tip (top electrode). There are two adsorption orientations between the TMA molecule and the metal electrodes in single-molecule junctions controlled by electrode potential in the experiment.[44] One is the TMA molecule lying flat on the Ni substrate called planar geometry, and the other is the TMA molecule standing upright on the Ni substrate called upright geometry. The planar geometry is shown in Fig. 1(a). Further considering the movement of the Ni tip in the experiment, three possible contact sites will be formed between the TMA molecule and the Ni tip. The pentagram, triangle, and circle symbols in the black dashed box in Fig. 1(a) indicate the position of the Ni tip in contact with the TMA molecule. The upright geometries are shown in Figs. 1(b) and 1(c), where the TMA molecule is sandwiched between the two Ni electrodes using carboxylic acids as anchoring groups. We have tested different adsorption sites (bridge, hollow, top) between the carboxylic acid group and the Ni substrate, where the most stable case is that the H atom is adsorbed at the bridge site and the double bonded O atom is adsorbed at the top site. As the Ni tip comes into contact with the carboxylic acid group, it may be located between the H atom and the double bonded O atom or directly above the double bonded O atom, corresponding to two upright geometries in Figs. 1(b) and 1(c), respectively.

The single-molecule junction as a whole can be divided into three parts: the central region, the semi-infinite top and bottom electrodes with fcc-(111) direction. The central region includes the TMA molecule as well as a partial top electrode (a tetrahedron tip composed of ten Ni atoms and three adjacent layers of Ni atoms) and bottom electrode (five layers of Ni atoms adjacent to the molecule). Except for the tip of the electrode, the remaining parts are described by 5×5 unit cell in X–Y plane with periodic boundary conditions. The electron transport is along the Z direction. According to the same or opposite magnetization directions of the two ferromagnetic electrodes, the single-molecule junctions can be manipulated into parallel (P) spin configuration or antiparallel (AP) spin configuration.

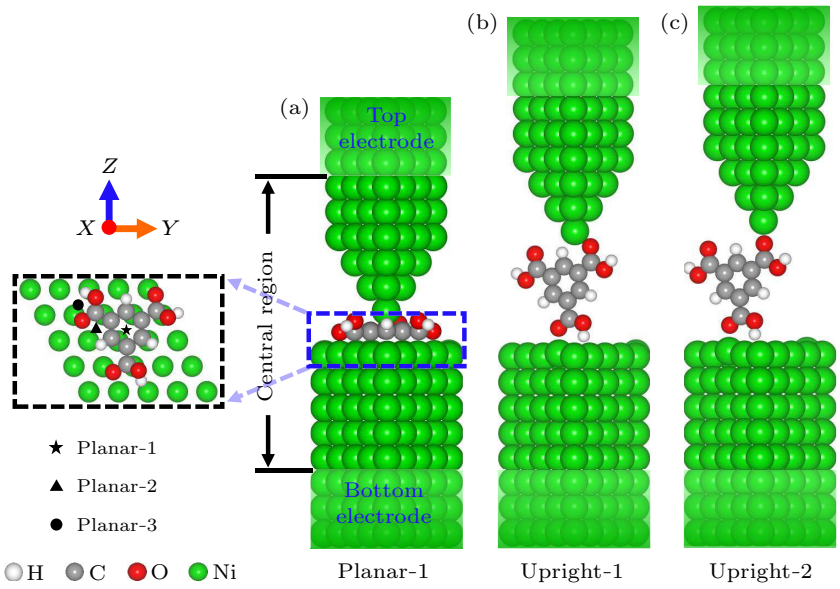


Fig. 1. Schematic of the Ni/TMA/Ni single-molecule junctions with different molecular adsorption orientations and electrode contact sites. (a) The TMA molecule is flat adsorbed on the nickel substrate electrode. The top view of contact details between TMA molecule and Ni tip electrode is shown in the black dashed box. According to the different sites of the tip electrode, these three configurations are named as planar-1, planar-2, and planar-3, respectively. [(b), (c)] The TMA molecules upright adsorbed on the substrate electrode.

The geometry optimization of single-molecule junctions and the following calculations of spin transport properties are executed in the Quantum ATK package[45,46] by using the density functional theory (DFT) combined with the nonequilibrium Green's function (NEGF) method.[47] During the geometry optimization, the maximum residual force on each atom is less than 0.04 eV/Å. The Troullier–Martins type norm-conserving pseudopotentials[48] are applied. The spin-dependent generalized gradient approximation (SGGA) with the Perdew–Burke–Ernzerhof (PBE) is used as the exchange–correlation functional.[49] The density mesh cutoff is set to 200 Ry. A double zeta (ζ) polarization (DZP) basis set is used for C, H, and O atoms, while a single zeta (ζ) polarization (SZP) is chosen for Ni atoms. The k-points of $3\times3\times100$ are adopted, corresponding to the X, Y, Z directions, respectively. The photons remain linearly polarized along the Z direction.

During the analysis of photocurrent, default values were used for the photocurrent parameters. The temperature is maintained at 300 K. The values of relative permittivity and relative permeability are set to 1. The photocurrent is obtained at the flux level of 1 $s^{-1}\cdot Å^{-2}$.

The spin-dependent current I under bias voltage V is calculated using the Landauer–Büttiker formula[50]

$$I_\sigma = \frac{e}{h}\int T_\sigma(E,V)[f_B(E-\mu_B)-f_T(E-\mu_T)]\mathrm{d}E, \quad (1)$$

where $\sigma = \uparrow / \downarrow$ represents the spin orientations of spin-up and spin-down electrons, $f_{B/T}(E-\mu_{B/T})$ is the Fermi–Dirac distribution function of electrons with energy E in bottom/top electrode, $\mu_{B/T}$ indicates the chemical potential of the bottom/top electrode. $T_\sigma(E,V)$ denotes the spin-dependent transmission spectrum, which is defined as

$$T_\sigma(E,V) = \mathrm{Tr}\left[\Gamma_\sigma^B(E,V)G_\sigma(E,V)\Gamma_\sigma^T(E,V)G_\sigma^+(E,V)\right]. \quad (2)$$

Here, $G_\sigma(E,V)/G_\sigma^+(E,V)$ represents the retarded/advanced Green's function of the central region. $\Gamma_\sigma^{B/T}(E,V)$ denotes the coupling matrix between the bottom/top electrode and the central region that takes into account the self-energies effect.

The spin-dependent photocurrent I in electrode α (bottom or top) with spin σ is calculated by[51–53]

$$I_{\alpha,\sigma} = \frac{e}{\hbar}\int \frac{\mathrm{d}E}{2\pi}\sum_k T_\sigma(E,k,\sigma). \quad (3)$$

The effective transmission coefficients are defined as[52]

$$T_\alpha(E,k,\sigma) = \mathrm{Tr}\{\mathrm{i}\Gamma_\alpha(E,k)[1-f_\alpha]G^< + f_\alpha G^>\}_{\sigma\sigma}. \quad (4)$$

Different from Eq. (2), Green's function $G^{>/<}$ in Eq. (4) includes electron–photon interactions to first order.

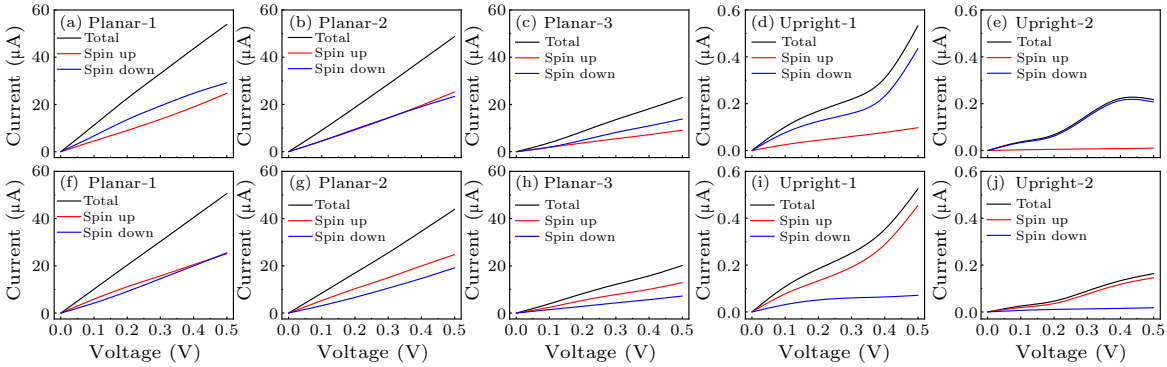


Fig. 2. (a)–(e) The total and spin-dependent current–voltage curves of planar and upright TMA molecular junctions in P spin configuration. (f)–(j) The ones in AP spin configuration.

3. Results and discussion

First, we investigate the conductivity of single-molecule junctions with different molecular adsorption orientations and electrode contact sites in P and AP spin configurations. The total and spin-dependent current–voltage curves are calculated as shown in Fig. 2. When the molecule lies flat on the substrate, the currents increase almost linearly with bias voltage regardless of the electrode contact sites under P and AP spin configurations shown in Figs. 2(a)–2(c) and 2(f)–2(h), respectively. However, the current gradually decreases as the Ni tip moves away from the benzene ring of the molecule. The total current of planar-1 junction is slightly higher than that of planar-2 junction, reaching a maximum value of over 50 μA at 0.5 V. When the Ni tip moves to the center of the carboxylic acid group, the total current of planar-3 junction rapidly decreases to a maximum value of only over 20 μA at 0.5 V. For upright geometry, as can be seen in Figs. 2(d)–2(e) and 2(i)–2(j), the total currents are two orders of magnitude lower than those of planar geometry. Our calculated total currents of the molecular junction formed by direct contact between the Ni electrodes and the π-system of the benzene ring are two orders of magnitude higher than the currents of the molecular junction where the benzene ring and Ni electrodes are connected by anchoring groups, which is consistent with the results re-

ported in previous experiments using Au electrode.[54] Therefore, the TMA single-molecule junctions with Ni electrodes also manifest the conductance switching behavior by manipulating the molecular adsorption orientation. The total currents of upright geometry also increase with the applied bias voltage below 0.4 V. More interestingly, the total current of upright-1 junction increases more sharply after 0.4 V, achieving the maximum value of over 0.5 μA at 0.5 V. On the contrary, the total current of upright-2 junction decreases with bias voltage above 0.4 V showing a negative differential resistance phenomenon, where the maximum total current is only over 0.2 μA at 0.4 V. The higher total current of upright-1 junction compared to that of upright-2 junction is caused by the Ni tip being far from the molecular backbone, which is consistent with the situation of planar geometry. In addition, it can be seen that the spin-up and spin-down currents of planar TMA molecular junctions are close to each other, exhibiting poor spin transport properties. However, the currents of the two spin directions in upright TMA molecular junctions have a significant difference, indicating the generation of high spin-polarized current.

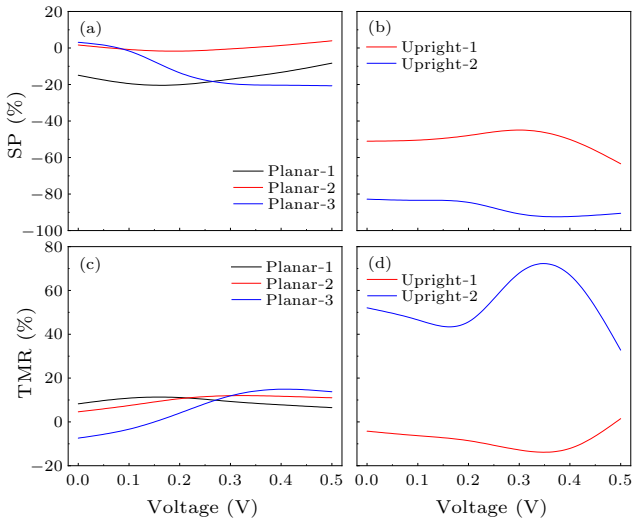


Fig. 3. The bias-dependent SP of current of (a) planar and (b) upright TMA molecular junctions in P spin configuration. The bias-dependent TMR of (c) planar and (d) upright TMA molecular junctions.

We next focus on the spin-dependent transport properties of planar and upright TMA molecular junctions. The SP of current of molecular junctions in P spin configuration is calculated as shown in Figs. 3(a) and 3(b). The SP of current under bias voltage V is defined by the equation $\mathrm{SP}(V) = [I_{\uparrow}(V) - I_{\downarrow}(V)]/[I_{\uparrow}(V) + I_{\downarrow}(V)] \times 100\%$, where $I_{\uparrow}(V)$ and $I_{\downarrow}(V)$ represent the current with spin-up and spin-down directions, respectively. To avoid zero current at zero bias voltage, the spin-dependent currents are replaced by the spin-dependent transmission coefficients at the Fermi level. As can be seen from Fig. 3(a), the SP of current of planar molecular junctions is kept at a low level throughout the calculated bias voltage range. The SP of current of planar-2 junction is almost zero in the bias range of 0.0–0.5 V. With the change of Ni tip position, planar-1 junction and planar-3 junction show negative SP of current in which the maximum value is only −20%. The SP of current of planar-1 junction decreases with bias voltage, while the SP of current of planar-3 junction increases with bias voltage. However, when the molecular orientation transforms from planar to upright, the SP of current significantly increases as shown in Fig. 3(b). For upright-1 junction, the SP of current stabilizes at −50% in the bias range of 0.0–0.4 V, and then grows to −65% at 0.5 V. In particular, upright-2 junction maintains extremely high SP of current of over 80% all over the investigated bias voltage range, even exceeding 90% after 0.3 V. Thus, compared with planar molecular junctions, upright molecular junctions have apparent SP of current, which can act as an optimal spin filter.

Then, the TMR of planar and upright molecular junctions under bias voltage V is also demonstrated in Figs. 3(c) and 3(d), which is evaluated as $\mathrm{TMR}(V) = [I_{\mathrm{P}}(V) - I_{\mathrm{AP}}(V)]/I_{\mathrm{AP}}(V) \times 100\%$. In the above equation, the $I_{\mathrm{P}}(V)$ and $I_{\mathrm{AP}}(V)$ represent the total current of P and AP spin configurations, respectively. Similarly, the total transmission coefficients at the Fermi level substitute for the total current under zero bias voltage. It is noted that the planar molecular junctions exhibit a terrible TMR effect in Fig. 3(c). As the position of the Ni tip changes, the TMR of planar-1 junction and planar-2 junction remains stable at around 10% within the 0.0–0.5 V bias voltage range. Furthermore, for planar-3 junction, the TMR first decreases with bias voltage from −10% and reverses at about 0.15 V, then increases to 15% at 0.4 V. In contrast, there is an evident difference in TMR between upright-1 and upright-2 junctions displayed in Fig. 3(d). For upright-1 junction, the TMR still stays a relatively low level similar to that of planar molecular junctions, which slowly increases from −4% to a maximum value of −13% in the bias range of 0–0.35 V and then decreases back to 0% in the bias range of 0.35–0.5 V. However, when the Ni tip comes into direct contact with the double bonded O atom, it is interesting to see that the TMR achieves a significant growth. The TMR of upright-2 junction oscillates with bias voltage, which first tends to decrease and then rises to a maximum value of about 70% around 0.35 V, and finally decreases again. Consequently, by controlling the contact sites between TMA molecule and Ni tip, an excellent TMR effect can be generated in upright geometry. In fact, compared with the currents of upright-1 and upright-2 junctions, the TMR effect is a more effective method to distinguish between the two configurations.

Now, the underlying physical mechanisms of the spin-dependent transport properties modulated by molecular adsorption orientations and contact sites between TMA molecule

and Ni tip are investigated. The spin-dependent projected density of states (PDOS) of the TMA molecule with planar and upright adsorption orientations in P spin configuration is plotted in Figs. 4(a) and 4(b). To label the position of molecular orbitals, the spin-dependent eigenvalues of molecular projected self-consistent Hamiltonian (MPSH)[55] are also marked. For planar molecular junctions, it can be seen that the PDOSs of the three molecules are intensely similar as shown in Fig. 4(a), especially near the Fermi level. The PDOSs exhibit continuous states jointly contributed by molecular orbitals and hybrid interface states in the vicinity of the Fermi level, which is indicative of a strong coupling between the TMA molecules with planar orientation and the Ni electrodes. However, when the molecular orientation transforms from planar to upright, the PDOS peaks become narrower and sharper in Fig. 4(b), suggesting that the TMA molecules are weakly coupled to Ni electrodes through carboxylic acids groups. According to the eigenvalues of MPSH, one can find that the PDOS peak closest to the Fermi level originates from the spin-down lowest unoccupied molecular orbital (LUMO). This is due to the fact that the interfacial coupling between the TMA molecule and Ni electrode in upright molecular junctions modifies the position of molecular orbitals so that the spin-down LUMO appears near the Fermi level and dominates charge transport. Moreover, in upright molecular junctions, the difference in the position of Ni tip changes the interfacial coupling between the TMA molecule and the top electrode, leading to different coupling strengths at the molecule/electrode interface. In upright-2 junction, the Ni tip is directly connected to the double bonded O atom of carboxylic acid group, causing the Ni tip to be further away from the molecular backbone relative to upright-1 junction, indicating a weaker coupling strength. This can be supported by the results of average effective potential of upright molecular junctions along z direction calculated in Fig. S1 of the supporting information. As shown in Fig. S1, the potential barrier at the contact interface between the TMA molecule and the Ni tip in upright-1 junction is -4.09 eV. However, the upright-2 junction possesses a much higher potential barrier of -3.66 eV at the molecule/electrode interface, which corresponds to a weaker coupling strength. As the coupling strength weakens, the attractive potential energy of electrons increases, leading to an increase in energy and a shift of molecular orbitals towards higher energy. The change in the position of Ni tip of upright-2 junction causes spin-up LUMO to move more energy than spin-down LUMO, resulting in a foreseeable high spin-down polarization near the Fermi level.

In order to see the variation of SP of the TMA molecule more clearly, the SP of the aforementioned molecular PDOS is calculated as shown in Figs. 4(c) and 4(d). The SP of molecular PDOS at energy E is defined as $\mathrm{SP}(E) = [\mathrm{PDOS}_{\uparrow}(E) - \mathrm{PDOS}_{\downarrow}(E)]/[\mathrm{PDOS}_{\uparrow}(E) + \mathrm{PDOS}_{\downarrow}(E)] \times 100\%$, where $\mathrm{PDOS}_{\uparrow}(E)$ and $\mathrm{PDOS}_{\downarrow}(E)$ represent the spin-up and spin-down PDOSs of molecules, respectively. In Fig. 4(c), it is noted that the SP of three planar molecules is overwhelmingly dreadful. The planar-1 and planar-2 molecules are almost spin-degenerated at the Fermi level, where the SP of planar-3 is only about 10%. This result means that the overpowering interface hybridization between the TMA molecule and the Ni electrodes does not lead to ideal SP of the molecule. In contrast, the two upright molecules show favorable spin-polarized phenomenon near the Fermi level. Especially, the SP of the TMA molecule in upright-2 junction has a significant increase to -50% at the Fermi level, which locates between an SP peak of -90% below the Fermi level and an SP peak of -60% above the Fermi level. As a result, upright molecular junctions have the ability to generate exceptional spin transport properties owing to the high SP of the molecules.

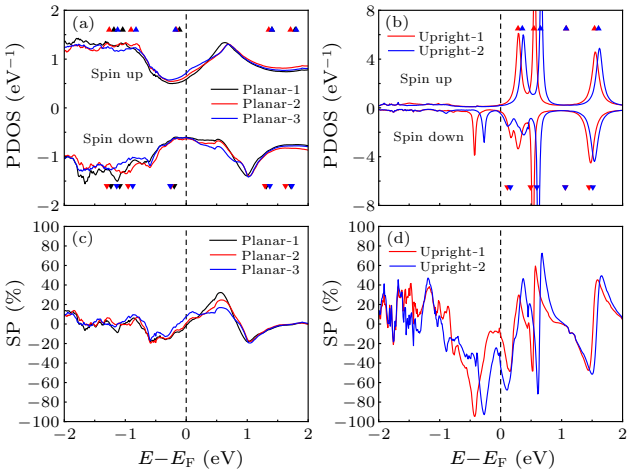


Fig. 4. Spin-dependent PDOS of the TMA molecule with (a) planar and (b) upright adsorption orientations in P spin configuration under zero bias voltage. The red and blue triangles are the spin-up and spin-down MPSH eigenvalues of the TMA molecule, respectively. The SP of the molecular PDOS with (c) planar and (d) upright adsorption orientations in P spin configuration under zero bias voltage.

In the following, we focus on the spin transport properties of upright molecular junctions and explore the relevant difference between the upright-1 and upright-2 junctions. The spin-dependent transmission spectra of the upright-1 and upright-2 molecular junctions in P and AP spin configurations under zero bias voltage are displayed in Fig. 5. As shown in Figs. 5(a) and 5(b), it is clearly seen that the transmission peak closest to the Fermi level is contributed by the spin-down LUMO, indicating that the PDOS peak provides effective transmission channels in P spin configuration. For upright-1 junction, the spin-down transmission coefficients are larger than the spin-up ones near the Fermi level. This corresponds to a higher spin-down current in Fig. 2(d) compared with the spin-up current, resulting in a spin-down SP of current

in Fig. 3(b). More importantly, the upright-2 junction is nearly insulating for the spin-up transmission around the Fermi level, and conducting for the spin-down transmission contributed by the tail of the spin-down LUMO peak. This results in the spin-up current being almost zero, while the spin-down current is at a certain value [see Fig. 2(e)]. Finally, a high SP of current about -90% is realized. It is noted that the upright-2 junction exhibits a significant decline of spin-down transmission peak at 0.15 eV, which brings about the weaker transmission capacity and lower current compared with the upright-1 junction. The results of AP spin configuration are given in Figs. 5(c) and 5(d). One can find that the spin-dependent transmission spectra of upright molecular junctions in AP spin configuration are basically antisymmetric to those in P spin configuration, where the spin-up and spin-down electrons flipped against each other. This is due to the weak interface coupling caused by the contact between TMA molecule and Ni substrate through the H atom on carboxylic acid group in upright molecular junctions, which causes that the magnetization direction of the Ni tip determines the SP of the TMA molecule. Therefore, when the magnetization direction of the Ni tip transitions from spin-up to spin-down into AP spin configuration, the SP of the TMA molecule is reversed. Furthermore, the total transmission coefficients of upright-1 junction under P and AP spin configurations are overwhelmingly similar near the Fermi level, which sparks off an unfavorable TMR effect. For upright-2 junction, there is a difference in the transmission coefficients near the Fermi level between the two spin configurations. The spin-up transmission peak at 0.1 eV in AP spin configuration is evidently lower than spin-down one in P spin configuration. Thus, the upright-2 junction enjoys a pleasurable positive TMR effect. To explain the mechanism of negative TMR in planar-3 and upright-1 TMA molecular junctions, the total transmission spectra of the two molecular junctions under zero bias voltage in P and AP spin configurations are given in Fig. S2. For planar-3 junction, the total transmission of P spin configuration near the Fermi level is vaguely lower than that of AP spin configuration, bringing about a weak negative TMR effect. For upright-1 junction, the total transmission of P and AP spin configurations is extremely close the value near the Fermi level. We drew the zoomed-in plots of total transmission spectra near the Fermi level and only then found that the total transmission of AP spin configuration is slightly higher than that of P spin configuration, which resulted in an overwhelmingly small negative TMR.

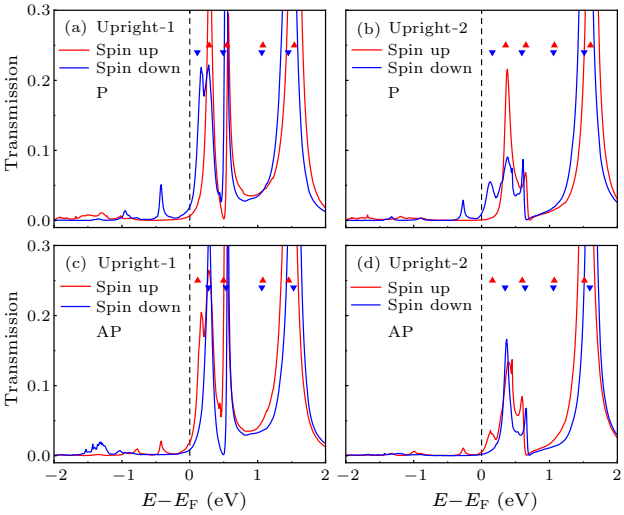


Fig. 5. Spin-dependent transmission spectra of the (a) upright-1 and (b) upright-2 molecular junctions in P spin configuration under zero bias voltage. [(c), (d)] The ones in AP spin configuration. The triangles are the spin-dependent MPSH eigenvalues of the TMA molecule. Red and blue lines indicate spin-up and spin-down currents, respectively.

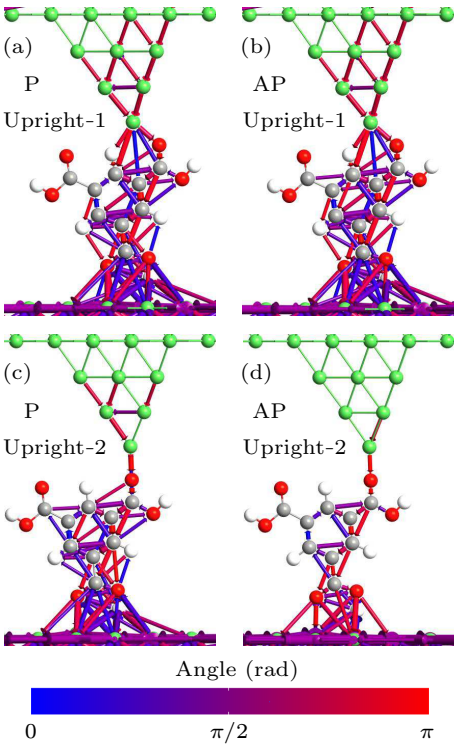


Fig. 6. The total transmission pathways of (a) upright-1 and (c) upright-2 molecular junctions at the Fermi level in P spin configuration under zero bias voltage. The cases in AP spin configuration are displayed in (b) and (d). Thresholds are fixed at 0.0003 for all plots.

To more intuitively see the situation of electron transmission, the total transmission pathways of upright-1 and upright-2 junctions at the Fermi level under zero bias voltage are given in Fig. 6. Electrons transport from the bottom electrode to the top electrode. The blue arrows and the red arrows indicate the transmission direction of electrons and the reflection direction of electrons, respectively. Thick arrows represent stronger transmission or reflection probability. It is clearly seen that there are intensely dense electron transmissions and reflec-

tions between the TMA molecule and the Ni substrate surface. For upright-1 junction, as shown in Figs. 6(a) and 6(b), electrons transmit to the top electrode through neighboring carbon atoms, and reflect back to the molecule through hydrogen and oxygen atoms in contact with the Ni apex atom. The electrons transmission pathways and the corresponding transmission probabilities in both P and AP spin configurations are almost identical, resulting in a little difference in currents of them and poor TMR effect. However, for upright-2 junction, electrons transport to top electrode through oxygen atoms depicted in Figs. 6(c) and 6(d). The electrons transmission is obviously suppressed in AP spin configuration, indicating a significant decrease in current. Thus, the TMR of upright-2 junction is radically enhanced compared with that of upright-1 junction.

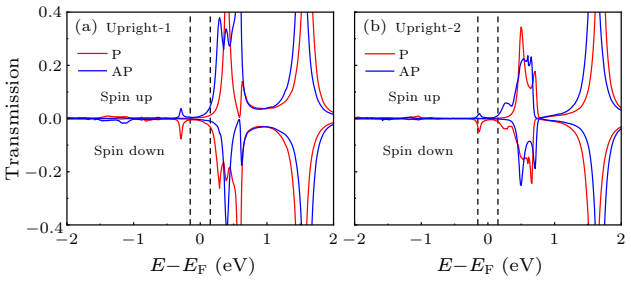


Fig. 7. Spin-dependent transmission spectra of the (a) upright-1 and (b) upright-2 molecular junctions at 0.3 V. The dashed lines indicate the bias window.

The spin-dependent transmission spectra of the two upright junctions in P and AP spin configurations at 0.3 V are plotted in Fig. 7. For upright-1 junction [Fig. 7(a)], one can find that the current is mainly contributed by the tail of the transmission peaks above the Fermi level in both P and AP spin configurations. In the bias window, the spin-up transmission probabilities of P spin configuration are smaller than the spin-down ones, leading to a moderate negative spin-polarized current of −45% at 0.3 V. At the same time, the total transmission probabilities of P and AP spin configurations are relatively close, which is responsible for the adverse TMR effect at 0.3 V. For upright-2 junction [Fig. 7(b)], two spin-down and spin-up transmission peaks below the Fermi level dominate the current in P and AP spin configurations, respectively. In the bias window, the spin-up transmission channel of P spin configuration is almost completely suppressed, which causes the SP of current reaches up to −90%. Moreover, it can be clearly seen that the total transmission probabilities of P spin configuration are significantly larger than those of AP spin configuration, bringing about a high positive TMR of about 70% at 0.3 V. As a result, the upright-2 junction has a more superior spin-filtering function as well as TMR effect compared with the upright-1 junction.

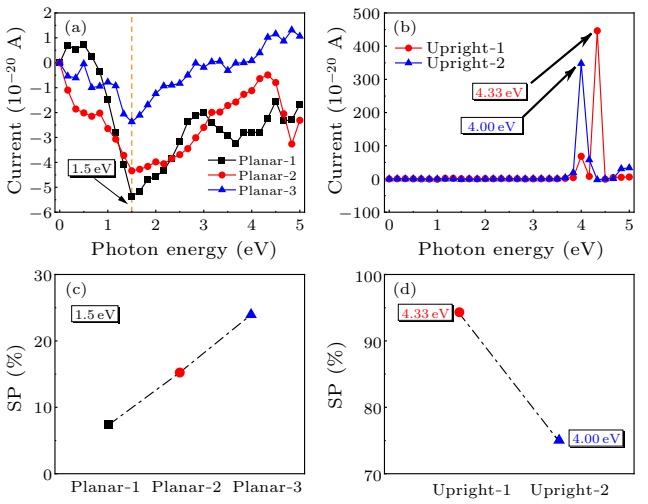


Fig. 8. The photocurrent of (a) planar and (b) upright TMA molecular junctions in P spin configuration under zero bias voltage with photon energy from 0 to 5 eV. The SP of photocurrent of (c) planar and (d) upright TMA molecular junctions at specific photon energy.

Finally, in order to investigate the photoelectric function of TMA molecular junctions, we have also calculated the photoresponse properties of TMA molecule under the irradiation of linearly polarized light along the Z direction. The variation of the photocurrent of planar and upright TMA molecular junctions with the incident light-polarized photon energy (wavelength) is given in Figs. 8(a) and 8(b), respectively. As shown in Fig. 8(a), all three planar molecular junctions generate photocurrent within the calculated photon energy range. The photocurrents of planar-1 junction and planar-2 junction are generally similar and both greater than that of planar-3 junction, which keep in the 10^{-20} A order of magnitude and reach the maximum value of no more than 5.5×10^{-20} A near 1.50 eV (826.7 nm). However, when the molecular adsorption configuration is transformed to upright, upright-1 and upright-2 junctions respectively exhibit a distinct sharp excitation peak near 4.33 eV (286.4 nm) and 4.00 eV (310.0 nm) manifested in Fig. 8(b), which are two orders of magnitude higher than the cases of planar molecular junctions. In contrast, the photocurrent of upright molecular junctions at other photon energies is extremely weak and is basically equivalent to that of planar molecular junctions, which is negligible compared to the photocurrent corresponding to the excitation peaks. In our calculations, the energy difference between the highest occupied molecular orbital (HOMO) and LUMO of the TMA molecule is 1.5 eV in planar molecular junctions, upright-1 and upright-2 junctions is 3.5 eV and 3.4 eV, respectively. It can be found that the photon energy corresponding to the excitation peak in planar molecular junctions is consistent with the molecular energy difference, while that in upright molecular junctions is greater than the molecular energy difference. The reason for this result is due to the fact that when flowing from the molecule to the electrode, the excited electrons

have to pass through the energy barrier related to the coupling strength between molecule and electrode, while the weaker coupling in upright molecular junctions requires more additional energy to cross the higher energy barrier. The upright molecular junctions have a better photoresponse to linearly polarized light along the Z direction than the planar molecular junctions. Thus, the stronger photoresponse of upright molecular junctions to different photon energies can be used to design and develop optoelectronic devices such as photosensitive sensors.

Figures 8(c) and 8(d) demonstrate the SP of photocurrent at the photon energy corresponding to the maximum excitation peak, which is defined as $\mathrm{SP}(\%) = \big||R_\uparrow| - |R_\downarrow|\big|/(|R_\uparrow| + |R_\downarrow|) \times 100$. $R_{\uparrow/\downarrow}$ represents the spin-up or spin-down photoresponse, which is proportional to the corresponding photocurrent at a luminous flux of 1 $\mathrm{s}^{-1}\cdot\mathrm{Å}^{-2}$. As shown in Fig. 8(c), it can be seen that the SP of photocurrent in planar molecular junctions is overwhelmingly low and the SP of photocurrent of the three molecular junctions planar-1, planar-2, and planar-3 increases sequentially. Nevertheless, there is a significant enhancement of the SP of photocurrent in upright molecular junctions displayed in Fig. 8(d). The SP of photocurrent of upright-1 junction is obviously higher than that of upright-2 junction, which reaches up to about 95%, tending to a fully spin-polarized photocurrent. Therefore, the intensity of photoresponse and the SP of photocurrent in TMA single-molecule junction are both closely related to the molecular adsorption configuration, where the upright molecular junctions can achieve the function of a favorable spin filter and photosensitive device related to illumination.

4. Conclusions

In summary, the spin-dependent transport properties and photoresponse characteristics of Ni/TMA/Ni magnetic single-molecule junction have been investigated by using the theoretical approaches based on DFT combined with the NEGF. The calculated results show that there is a conductance switch of two orders of magnitude with respect to the molecular adsorption orientation changing from planar geometry to upright geometry. In addition, the SP of current of upright molecular junctions is significantly higher than that of planar molecular junctions, which can reach up to -90% in upright-2 junction. More importantly, in upright molecular junction, changing the contact site between the Ni tip and the TMA molecule can achieve a stable TMR switch. A TMR up to 70% is obtained in upright-2 junction. The analysis of the spin-dependent PDOS reveals the TMA molecule in upright-2 junction has the highest SP, resulting in an excellent SP of current. The large difference in the electron transmission pathways of the P and AP spin configurations in upright-2 junction is intrinsically responsible for the ideal TMR effect. Furthermore, upright molecular junctions exhibit better photoresponse characteristics than planar molecular junctions. The maximum photocurrent of upright molecular junctions is two orders of magnitude higher than that of planar molecular junctions. Meanwhile, the SP of photocurrent has a significant enhancement in upright molecular junctions. As a result, anisotropic transport properties can be realized by manipulating the molecular adsorption direction and electrode contact sites in TMA molecular junctions. Our work proposes a reliable method for designing efficient molecular spintronic devices and optoelectronics devices using anisotropic molecule.

Acknowledgments

Project supported by the National Natural Science Foundation of China (Grant Nos. 11974217, 12204281, and 21933002) and the Shandong Provincial Natural Science Foundation (Grant No. ZR2022QA068).

References

[1] Naber W J M, Faez S and Wiel W G V D 2007 *J. Phys. D: Appl. Phys.* **40** R205
[2] Lv X R, Liang S H, Tao L L and Han X F 2014 *Spin* **4** 1440013
[3] Sanvito S 2011 *Chem. Soc. Rev.* **40** 3336
[4] Hirohata A, Yamada K, Nakatani Y, Prejbeanu I L, Diény B, Pirro P and Hillebrands B 2020 *J. Magn. Magn. Mater.* **509** 166711
[5] Guo L, Qin Y, Gu X, Zhu X, Zhou Q and Sun X 2019 *Front. Chem.* **7** 428
[6] Miao Y, Qiu S, Zhang G, Ren J, Wang C and Hu G 2018 *Phys. Rev. B* **98** 235415
[7] Rocha A R, García-Suárez V M, Bailey S W, Lambert C J, Ferrer J and Sanvito S 2005 *Nat. Mater.* **4** 335
[8] Sun D, Ehrenfreund E and Vardeny Z V 2014 *Chem. Commun.* **50** 1781
[9] Barraud C, Seneor P, Mattana R, Fusil S, Bouzehouane K, Deranlot C, Graziosi P, Hueso L, Bergenti I, Dediu V, Petroff F and Fert A 2010 *Nat. Phys.* **6** 615
[10] Cinchetti M, Dediu V A and Hueso L E 2017 *Nat. Mater.* **16** 507
[11] Raman K V, Kamerbeek A M, Mukherjee A, Atodiresei N, Sen T K, Lazić P, Caciuc V, Michel R, Stalke D, Mandal S K, Blügel S, Münzenberg M and Moodera J S 2013 *Nature* **493** 509
[12] Sanvito S 2010 *Nat. Phys.* **6** 562
[13] Galbiati M, Tatay S, Barraud C, Dediu A V, Petroff F, Mattana R and Seneor P 2014 *MRS Bull.* **39** 602
[14] Liang S H, Liu D P, Tao L L, Han X F and Guo H 2012 *Phys. Rev. B* **86** 224419
[15] Sun M and Mi W 2018 *J. Mater. Chem. C* **6** 6619
[16] Gao F, Li D, Barreteau C and Brandbyge M 2022 *Phys. Rev. Lett.* **129** 027201
[17] Lach S, Altenhof A, Tarafder K, Schmitt F, Ali M E, Vogel M, Sauther J, Oppeneer P M and Ziegler C 2012 *Adv. Funct. Mater.* **22** 989
[18] Shi S, Sun Z, Bedoya-Pinto A, Graziosi P, Li X, Liu X, Hueso L, Dediu V A, Luo Y and Fahlman M 2014 *Adv. Funct. Mater.* **24** 4812
[19] Guo L, Gu X, Zhu X and Sun X 2019 *Adv. Mater.* **31** 1805355
[20] Delprat S, Galbiati M, Tatay S, Quinard B, Barraud C, Petroff F, Seneor P and Mattana R 2018 *J. Phys. D: Appl. Phys.* **51** 473001
[21] Kawahara S L, Lagoute J, Repain V, Chacon C, Girard Y, Rousset S, Smogunov A and Barreteau C 2012 *Nano Lett.* **12** 4558
[22] Dalgleish H and Kirczenow G 2006 *Phys. Rev. B* **73** 245431
[23] Qiu S, Miao Y Y, Zhang G P, Ren J F, Wang C K and Hu G C 2020 *J. Phys. Chem. C* **124** 12144
[24] Zhang N, Lo W Y, Cai Z, Li L and Yu L 2017 *Nano Lett.* **17** 308
[25] Zhang G P, Mu Y Q, Wei M Z, Wang S, Huang H, Hu G C, Li Z L and Wang C K 2018 *J. Mater. Chem. C* **6** 2105

[26] Tao L L and Wang J 2017 *Nanoscale* **9** 12684

[27] Li D, Banerjee R, Mondal S, Maliyov I, Romanova M, Dappe Y J and Smogunov A 2019 *Phys. Rev. B* **99** 115403

[28] Goren N, Das T K, Brown N, Gilead S, Yochelis S, Gazit E, Naaman R and Paltiel Y 2021 *Nano Lett.* **21** 8657

[29] Cardona-Serra S, Gaita-Ariño A, Stamenova M and Sanvito S 2017 *J. Phys. Chem. Lett.* **8** 3056

[30] Zhang X, Tong J, Zhu H, Wang Z, Zhou L, Wang S, Miyashita T, Mitsuishi M and Qin G 2017 *J. Mater. Chem. C* **5** 5055

[31] Yao X, Duan Q, Tong J, Chang Y, Zhou L, Qin G and Zhang X 2018 *Materials* **11** 721

[32] Vezzoli A, Brooke R J, Higgins S J, Schwarzacher W and Nichols R J 2017 *Nano Lett.* **17** 6702

[33] Han X, Mi W and Wang X 2019 *J. Mater. Chem. C* **7** 4079

[34] Zhou Y, Yu S and Zheng X 2020 *Carbon* **170** 361

[35] Chen J, Zhang L, Zhang L, Zheng X, Xiao L, Jia S and Wang J 2018 *Phys. Chem. Chem. Phys.* **20** 26744

[36] Michnowicz T, Borca B, Pétuya R, Schendel V, Pristl M, Pentegov I, Kraft U, Klauk H, Wahl P, Mutombo P, Jelínek P, Arnau A, Schlickum U and Kern K 2020 *Angew. Chem. Int. Ed.* **59** 6207

[37] Herrer I L, Ismael A K, Milán D C, Vezzoli A, Martín S, González-Orive A, Grace I, Lambert C, Serrano J L, Nichols R J and Cea P 2018 *J. Phys. Chem. Lett.* **9** 5364

[38] Wang Y H, Zhou X Y, Sun Y Y, Han D, Zheng J F, Niu Z J and Zhou X S 2014 *Electrochim. Acta* **123** 205

[39] Li X M, Wang Y H, Seng J W, Zheng J F, Cao R, Shao Y, Chen J Z, Li J F, Zhou X S and Mao B W 2021 *ACS Appl. Mater. Interfaces* **13** 8656

[40] Zhu Z, Qu H, Chen Y, Zhang C, Li R, Zhao Y, Zhou Y, Chen Z, Liu J, Xiao Z and Hong W 2021 *J. Mater. Chem. C* **9** 16192

[41] Gao T, Pan Z, Cai Z, Zheng J, Tang C, Yuan S, Zhao S, Bai H, Yang Y, Shi J, Xiao Z, Liu J and Hong W 2021 *Chem. Commun.* **57** 7160

[42] Yasini P, Afsari S, Peng H, Pikma P, Perdew J P and Borguet E 2019 *J. Am. Chem. Soc.* **141** 10109

[43] Pal A N, Li D, Sarkar S, Chakrabarti S, Vilan A, Kronik L, Smogunov A and Tal O 2019 *Nat. Commun.* **10** 5565

[44] Afsari S, Yasini P, Peng H, Perdew J P and Borguet E 2019 *Angew. Chem. Int. Ed.* **58** 14275

[45] Soler J M, Artacho E, Gale J D, García A, Junquera J, Ordejón P and Sánchez-Portal D 2002 *J. Phys.: Condens. Matter* **14** 2745

[46] Atomistix ToolKit version2018.06, Synopsys QuantumWise A/S (www.quantumwise.com).

[47] Brandbyge M, Mozos J L, Ordejón P, Taylor J and Stokbro K 2002 *Phys. Rev. B* **65** 165401

[48] Troullier N and Martins J 1990 *Solid State Commun.* **74** 613

[49] Perdew J P, Burke K and Ernzerhof M 1997 *Phys. Rev. Lett.* **77** 3865

[50] Büttiker M, Imry Y, Landauer R and Pinhas S 1985 *Phys. Rev. B* **31** 6207

[51] Chen J, Hu Y and Guo H 2012 *Phys. Rev. B* **85** 155441

[52] Henrickson L E 2002 *J. Appl. Phys.* **91** 6273

[53] Zhang L, Gong K, Chen J, Liu L, Zhu Y, Xiao D and Guo H 2014 *Phys. Rev. B* **90** 195428

[54] Afsari S, Li Z and Borguet E 2014 *Angew. Chem. Int. Ed.* **53** 9771

[55] Larade B, Taylor J, Zheng Q R, Mehrez H, Pomorski P and Guo H 2001 *Phys. Rev. B* **64** 195402